Chapitre 7 :

Ségrégation de phases, hétérogénéité magnétique et désordre : $Pr_{2/3}Ca_{1/3}MnO_3$.

7 Ségrégation de phases, inhomogénéité magnétique et désordre : $Pr_{2/3}Ca_{1/3}MnO_3$

Dans le chapitre suivant, nous présentons une étude sur la nature in homogène de l'état d'ordre de charge dans $Pr_{1-x}Ca_xMnO_3$ avec x=1/3 basé sur des expériences de NPD et les mesures de magnétisation sous champs magnétiques élevés et sur des mesures de relaxation de muons (µSR). Cette étude contribue à la description et à la compréhension plus précise des phénomènes de ségrégation de phase et de la distribution spatiale des phases qui coexistent (FM/Métallique et CO/Isolante) dans ce composé. Une étude comparative a été réalisée avec le composé à ordre de charge $Pr_{1/2}Ca_{1/2}MnO_3$.

7 Phase segregation, magnetic inhomogeneity and disorder in $Pr_{2/3}$ $Ca_{1/3}MnO_3$

In the following chapter, we present a study on the non homogeneous nature of the CO state in $Pr_{1-x}Ca_xMnO_3$ with x=1/3 based on NPD experiments and magnetisation measurements under high magnetic fields and on muon spin relaxation (μSR). This study contributes to the more precise description and understanding of the phase segregation phenomena and spatial distribution of the coexisting FM/Metallic and CO/Insulating phases in this compound. A comparative study has been performed with the CO $Pr_{1/2}Ca_{1/2}MnO_3$ compound.

7.1 Introduction

Phase segregation (PS) phenomena has recently been discovered as being an important issue in manganites [151]. Early works of De Gennes already hypothesised the possibility of phase coexistence in manganese oxides and recently, theoretical studies have concluded that some charge densities could not be stabilised in manganites [159]. Hence, at certain charge concentrations the ground state is expected to be inhomogeneous with two coexisting phases: one FM and metallic and the other insulating. This type of phase segregation is expected to be electronically driven and the FM/metallic phase is expected to be short range (10-30Å) due to the high Coulomb energy cost of the electronic separation.

There exist experimental evidence of phase segregation in manganite based compounds for different carrier concentrations [151]. We have chosen the $Pr_{2/3}Ca_{1/3}MnO_3$ ($<r_A>$=1.12Å) as the object of our study because it is in the border line between relatively large bandwidth compounds that give FM and metallic ground states as is the case of $La_{2/3}Ca_{1/3}MnO_3$ compound ($<r_A>$=1.15Å), and insulating compounds without long range magnetic order as in $La_{0.35}Y_{0.35}Ca_{0.3}MnO_3$ ($<r_A>$=1.10Å). In addition, as the ionic radii of Ca^{+2} and Pr^{+3} is very similar, a change in the Ca content do not change the ionic variance.

Upon cooling, $Pr_{2/3}Ca_{1/3}MnO_3$ presents a charge ordering transition at T_{CO}=200K which is accompanied with an AFM order at T_N=150K. The most unexpected features in this compound are: a) the AFM order which corresponds to a CE-type which is usually associated to x=1/2 doped compounds, and b) the transition occurring at lower temperatures (≈100K) when the compound is in the AFM state, where a net FM moment appears.

The low temperature configuration was firstly described with a CE-type magnetic structure with a FM canting below 100K [160]. However, it has been recently reported the induction of phase

segregation in this compound under the exposure to X-Rays at low temperatures [161, 162]. The induced FM new phase persists after the X-Rays are switched off and only disappears upon warming above 40K. Other experiments showed that upon the application of an external magnetic field, an insulator-to metal transition was also induced and the metallic state persisted when the magnetic field was turned to zero [163]. This metastable and phase segregated state was studied also by relaxation studies on the transport measurements [164]. These studies concluded that the metallic and FM induced state exhibits thermally activated relaxation phenomena towards an insulating state.

The low temperature FM and metallic state has been also stabilised under the application of electric fields [165], hydrostatic pressure [166], electron beam exposure[167], irradiation with laser pulses [168]or visible light [169].

In the following sections the macroscopic properties of $Pr_{1-x}Ca_xMnO_3$ compounds with x=1/2 and x=1/3 are presented. The most relevant features in these compounds are interpreted on the light of microscopic techniques as μSR and high resolution NPD.

7.2 $Pr_{2/3}Ca_{1/3}MnO_3$ vs $Pr_{1/2}Ca_{1/2}MnO_3$

Polycrystalline $Pr_{1/2}Ca_{1/2}MnO_3$ and $Pr_{2/3}Ca_{1/3}MnO_3$ ceramic samples were prepared by conventional solid state reaction. A mixture of $CaCO_3$, Mn_2O_3 and Pr_6O_{11} at the desired ratio was prefired at 750°C in air. After some intermediate treatments, the powders were pressed into pellets, fired at 1400°C for 15h, cooled to room temperature and ground again for several times. The sample preparation was performed at the ICMAB synthesis laboratory.

7.2.1 Orbital and Charge Ordering in $Pr_{1/2}Ca_{1/2}MnO_3$

$Pr_{12}Ca_{1/2}MnO_3$ is an example of the development of orbital and charge ordering in x=1/2 compounds[2] which present the CE-type magnetic structure at low temperatures. The OO, CO and CE type magnetic structure in x=1/2 compounds have been shown to be sensitive to the different annealing conditions and oxygen stoichiometry [170, 171]. When disorder due to slight off stoichiometry of the Mn^{+3}/Mn^{+4}:1 ratio exist, the low temperature CE-type AFM magnetic structure develops FM coupling between the AFM planes (in the *c* direction in the Pbnm setting) giving rise to the so called pseudo-CE magnetic structure.

[2] In this thesis we always use the pure ionic picture of the charge ordering even if very recent works seem to show a certain degree of covalence in this orbitally ordered states (J. Rodriguez-Carvajal private communication)

In the following section the stabilisation of the CE-type magnetic order and of the CO is described from NPD data analysis in the $Pr_{1/2}Ca_{1/2}MnO_3$ compound.

7.2.1.1 Neutron Powder Diffraction study

$Pr_{1/2}Ca_{1/2}MnO_3$ compound was studied using NPD data obtained at different temperatures between 1.5K to 300K using the high intensity D1B diffractometer (λ=2.52Å) at ILL.

At 300K, the $Pr_{1/2}Ca_{1/2}MnO_3$ compound is a paramagnetic insulator and its crystallographic structure can be satisfactorily indexed using an orthorhombic Pbnm space group (a=5.3954(7)Å, b=5.4054(7)Å, c=7.6058(9)Å).

In Fig. 7-1 is shown the thermal evolution of the NPD patterns of $Pr_{12}Ca_{1/2}MnO_3$ obtained at D1B diffractometer at ILL (Grenoble). At 230K it can be observed the reduction of the intensity of some structural Bragg peaks due to the splitting of several reflections. Below 180K, new peaks appear at low angles and have been identified to correspond to a CE-type magnetic structure.

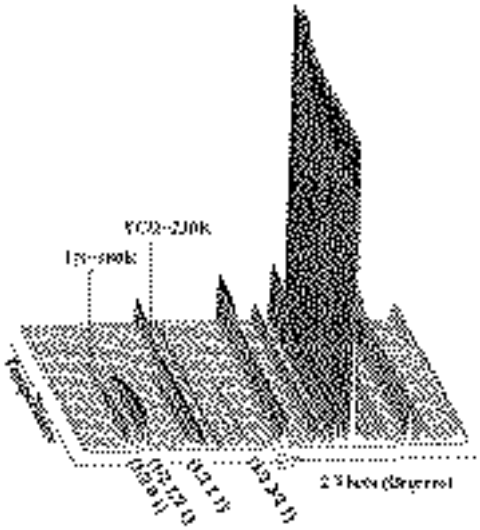

Fig. 7-1 *Thermal evolution of the NPD patterns showing the structural transition of the $Pr_{1/2}Ca_{1/2}MnO_3$ compound at T_{CO}=230K and the onset of AFM order at T_N=180K.*

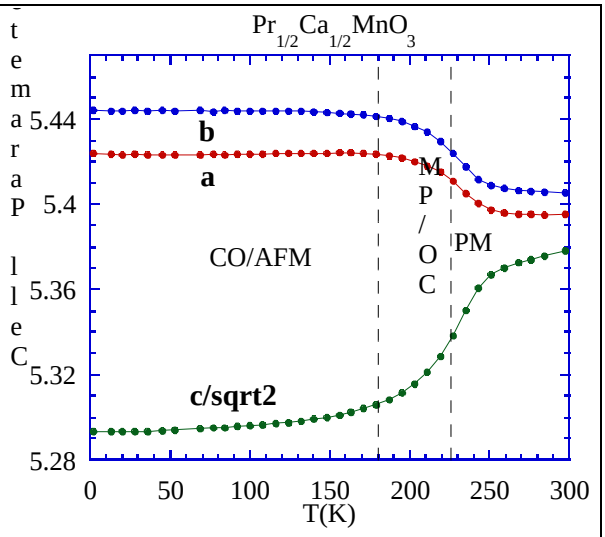

Fig. 7-2 *Thermal evolution of the lattice parameters of the $Pr_{1/2}Ca_{1/2}MnO_3$ compound in the Pbnm setting obtained from NPD Rietveld analysis.*

The analysis of the thermal evolution of the cell parameters from our NPD data reveals that upon cooling, there is an anisotropic structural transition (Fig. 7-2). This transition at 230K has been identified to be the CO transition. At this temperature a particular OO stabilises due to the localisation of the e_g electrons in the real space. Below this temperature appears a peak which could not be indexed on the basis of the lattice obtained at RT. This peak can be indexed as (2 1/2 2) or which means that the unit cell is doubled in the (0 1 0) direction. Its thermal evolution is presented in Fig. 7-3. The number of observed

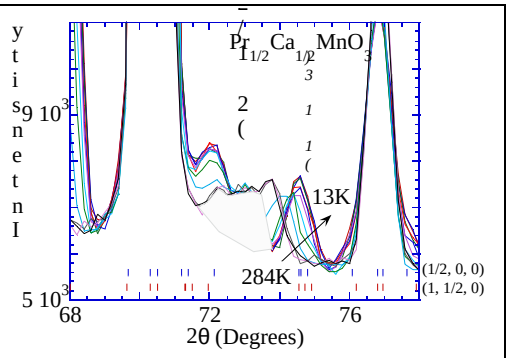

Fig. 7-3 *Thermal evolution of the (2 1/2 2) superstructure peak in $Pr_{1/2}Ca_{1/2}MnO_3$ in the temperature range between 284K to 13K. The shaded region corresponds to signal comming from the cryostat that does not evolve with temperature.*

superstructure peaks is low in our NPD data, hence, we will describe the OO superstructure by its averaged cell. At 1.5K the NPD pattern can still be indexed using the averaged Pbnm unit cell (a=5.4238(6)Å, b=5.4443(5)Å, c=7.4860(8)Å).

The orbital order appearing at 230K is consistent with Goodenough [17] early studies and consists in the stacking of planes with $d_z^2Mn^{+3}$ orbitals ordered in such a way as to form zig-zag chains in the plane (Fig. 7-5). Such OO will originate an expansion of the cell parameters in the plane containing the $d_z^2Mn^{+3}$ ordered orbitals and a reduction of the cell parameter perpendicular to these planes. The inspection of the thermal evolution of the cell parameters of $Pr_{1/2}Ca_{1/2}MnO_3$ as extracted from our NPD data (Fig. 7-2), suggests that the Mn^{+3} d_z^2 orbitals lay in the *ab* plane in the Pbnm description of the structural cell. The development of such OO generates a superstructure that develops through the doubling of one of the in-plane cell parameters. So, when long range OO stabilises, there appear superlattice peaks, which cannot be indexed with a simple $a=\sqrt{2}\ a_p$, $b=\sqrt{2}\ a_p$, $c=2\ a_p$ cell (a_p corresponds to the primitive perovskite lattice parameters) but with a a×2b×c cell.

Below T_N=180K an AFM structure develops which corresponds to the CE-type AFM ordering which is consistent with the Mn^{+3} and Mn^{+4} ions being ordered in the real space (Fig. 7-5). In such magnetic structure, the propagation vectors are different for Mn^{+3} ([1/2,0,0]) and Mn^{+4} ([1/2,1/2,0]) in Pbnm setting). The refinement of the magnetic structure using the CE type ordering is shown in Fig. 7-4. It converged to different magnetic moment (mainly oriented in the *ab* plane) for the two different sites of Mn ion (Tab. 7-I):

a) Mn(I) position (0.25, 0, 0) and m=2.9(2)μ_B/Mn propagation vector [1/2,0,0]

b) Mn(II) position (0,0.25,0) and m=2.6(2)μ_B/Mn propagation vector [1/2,1/2,0]

Hence Mn(I) can be associated with Mn^{+3} and Mn(II) with Mn^{+4} ions. It can be observed that the magnetic peaks associated to Mn^{+3} ions are broader than those associated to Mn^{+4} which has been associated to the existence of antiphase boundaries in the Mn^{+3} magnetic structure [172].

In 1955 [20]and [17] proposed that the CE type magnetic structure could be constructed from the charge-ordered structure when assuming that the Mn-O-Mn superexchange interactions are FM when one of the Mn-O bonds are short.

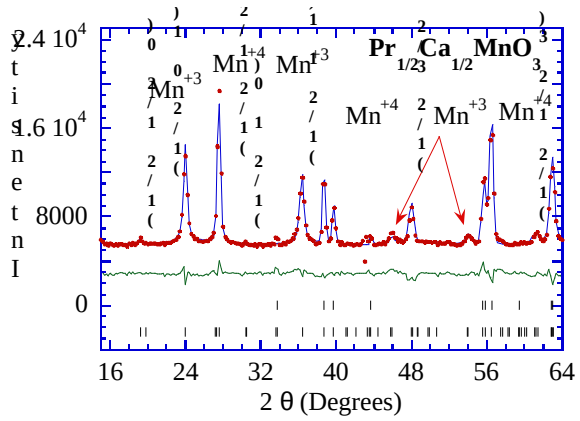

Fig. 7-4 *Detail of the NPD low angle region of the $Pr_{1/2}Ca_{1/2}MnO_3$ at 1.5K showing the AFM peaks corresponding to the CE type magnetic order.*

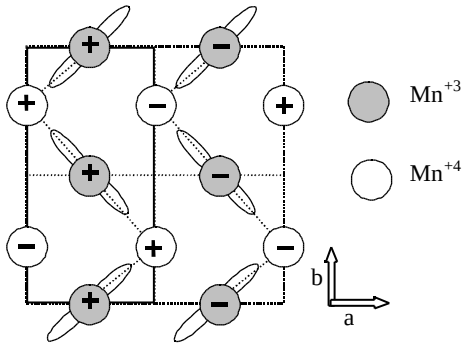

Fig. 7-5 *Schematic image of the CE-type magnetic and orbital order.*

Tab. 7-I. Results of the magnetic refinement of the NPD data on $Pr_{1/2}Ca_{1/2}MnO_3$ (R_{mag}=10)			
Mn^{+3}= 2.9(2)		Mn^{+4}=2.6 (2)	
Site	(2.6(2),1.3(2),0.5(1))μ_B/Mn	Site	(-1.7(4),-1.9(4),-0.4(1))μ_B/Mn
(1/4,0,0)	+1 +1 +1	(0,1/4,0)	+1 +1 +1
(3/4,0,0)	-1 -1 -1	(1/2,1/4,0)	-1 -1 -1
(1/4,1/2,0)	+1 +1 +1	(0,3/4,0)	-1 -1 -1
(3/4,1/2,0)	-1 -1 -1	(1/2,3/4,0)	+1 +1 +1
(1/4,0,1/2)	-1 -1 +1	(0,1/4,1/2)	-1 -1 +1
(3/4,0,1/2)	+1 +1 -1	(1/2,1/4,1/2)	+1 +1 -1
(1/4,1/2,1/2)	-1 -1 +1	(0,3/4,1/2)	+1 +1 -1
(3/4,1/2,1/2)	+1 +1 -1	(1/2,3/4,1/2)	-1 -1 +1

In next section, we present the results of magnetisation and resistivity measurements characterising the CO state on $Pr_{1/2}Ca_{1/2}MnO_3$ compound.

7.2.1.2 Magnetic and resistivity characterisation

From the macroscopic point of view, at the charge ordering transition (T_{CO}≈230K) there is a reduction of the magnetisation of the sample as shown in Fig. 7-6. In $Ln_{1/2}Ca_{1/2}MnO_3$ compounds exhibiting charge-ordering state, the magnetisation of the sample decreases when the sample is cooled down through the CO transition and θ_C changes its sign from positive to negative. The reason is the substitution of the FM correlation by AFM ones that is concomitant with the orbital ordering.

The application of magnetic fields up to 10T on $Pr_{1/2}Ca_{1/2}MnO_3$ are unable to break the AFM and CO state in $Pr_{1/2}Ca_{1/2}MnO_3$. Nevertheless, the application of a magnetic field modifies T_{CO} because the magnetic field favours the FM metastable state but longer fields are required to stabilise the FM. No feature is observed at T_N≈180K in magnetisation measurements.

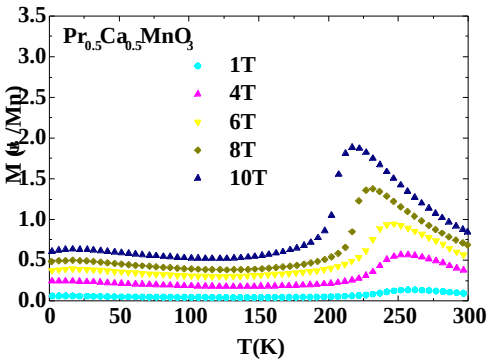

.

Fig. 7-6 *Magnetisation measurements on $Pr_{12}Ca_{1/2}MnO_3$ polycrystalline sample displaying the diminution of magnetisation at T_{CO}≈230K .*

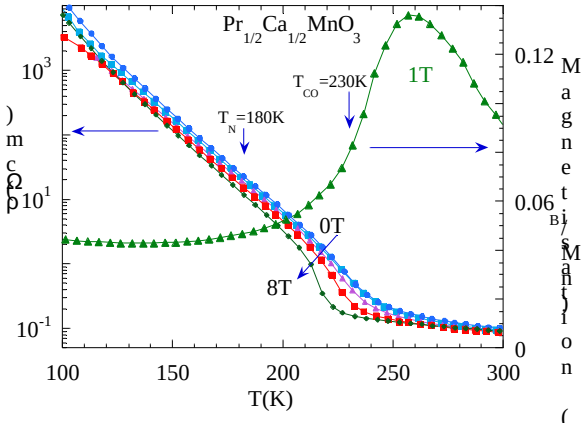

Fig. 7-7 *Resistivity measurements at several applied magnetic fields on $Pr_{1/2}Ca_{1/2}MnO_3$ compound and magnetisation measurement at 1T*

Resistivity measurements performed using the four-probe method on a polycrystalline ceramic sample at several applied magnetic fields on $Pr_{1/2}Ca_{1/2}MnO_3$ compound are also shown in Fig. 7-7. It can be observed that, at $T_{CO,}$ there is a decrease of the magnetisation of the sample at the same time that the resistivity exhibits a kink indicating the onset of the carrier localisation. In addition, while there is no sign of the onset of AFM order in the magnetisation measurements, there exists an upturn in the electrical resistivity indicating a change in the magnetic state of the sample (Fig. 7-8).

In conclusion, the $Pr_{1/2}Ca_{1/2}MnO_3$ sample, is a paradigmatic case that displays the structural transition originated by the concomitant orbital order and the ordered localisation of the carriers in the real space. At temperatures lower than T_{CO}≈230K and OO transition, a CE-type magnetic structure develops with the magnetic moments mainly in the *ab* plane (T_N≈180K).

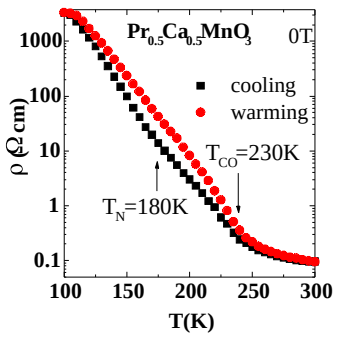

Fig. 7-8 Zero field resistivity measurements upon cooling and warming displaying anomalies at T_{CO} and T_N

7.2.2 Magnetic inhomogeneity and disorder of $Pr_{2/3}Ca_{1/3}MnO_3$

As has been described in the introduction of this chapter, $Pr_{2/3}Ca_{1/3}MnO_3$ exhibits a series of unexpected structural and magnetic transitions and there are some evidences of the existence of phase separation phenomena at low temperatures. The origin of these states can be the similar energy of the competing states responsible for the FM-AFM order. This fact is reflected in the phase diagram of $Pr_{1-x}Ca_xMnO_3$ shown in Fig. 7-9. At low temperatures, the x=1/3 compound is in the borderline between FM-Insulating (x<1/3) and AFM-Insulating states (x>0.4).

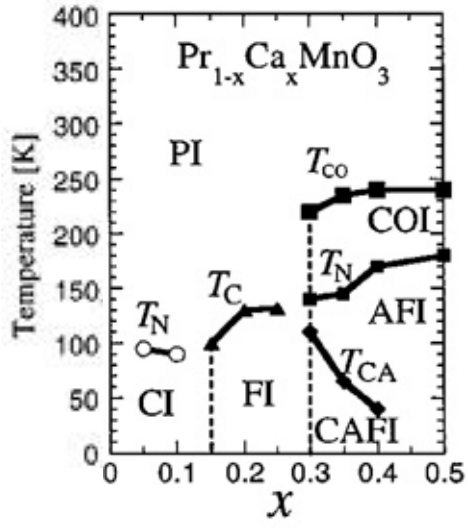

Fig. 7-9 *Phase diagram of $Pr_{1-x}Ca_xMnO_3$ extracted from [163]*

In addition, $Pr_{2/3}Ca_{1/3}MnO_3$ compound is representative of the intermediate-x region in samples of a moderate distortion (bandwidth placed close to the boundary that separates metallic and insulating low-temperature behaviour).

Magnetisation measurements under low magnetic fields, after zero field cooling (ZFC) and 2mT field cooling (FC) on $Pr_{2/3}Ca_{1/3}MnO_3$ polycrystalline sample display a small sign of the CO transition approximately at 220K as shown in the inset of (Fig. 7-10). At variance with $Ln_{1/2}Ca_{1/2}MnO_3$ compounds exhibiting CO at low temperatures, $Pr_{2/3}Ca_{1/3}MnO_3$ displays no change in the sign of θ_C below and above T_{CO} ($\theta_c(T>T_{CO})\approx 170K$, $\theta_C(150K<T<T_{CO})\approx 110K$).

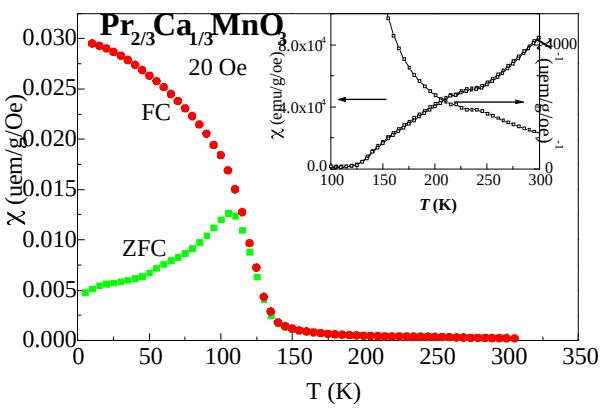

Fig. 7-10 *Magnetisation under 2mT Oe after ZFC and FC for $Pr_{2/3}Ca_{1/3}MnO_3$ polycrystalline sample. In the inset a detail of the dc susceptibility is shown displaying a small change at T_{CO}.*

At 100K, a hysteretic behaviour appears between the FC and ZFC measurements and the FC measurement displays a saturation value which is six times the value obtained at ZFC. The temperature at the onset of the hysteretic behaviour corresponds to the temperature where the net FM moment is observed in our NPD data.

7.2.3 $Pr_{2/3}Ca_{1/3}MnO_3$: A Neutron Powder Diffraction study

NPD measurements were performed on $Pr_{2/3}Ca_{1/3}MnO_3$ polycrystalline sample using the diffractometers D1B (λ=2.52Å) at ILL(Grenoble) and G4.1(λ=2.426Å) at Lab. Leon Brillouin (Saclay). The thermal evolution of the diffraction patterns (Fig. 7-11) evidences the apparition of peaks at low angles associated to the AFM ordering at temperatures below T_N≈150K.

At 220K, slightly above T_{CO}≈200K, the NPD data is well indexed using an orthorhombic cell with the space group Pbnm (a=5.433(1)Å, b=5.464(1)Å, c=7.667(1)Å). The analysis of the NPD data at different temperatures reveals that upon cooling through T_{CO} no abrupt structural changes are observed (Fig. 7-13) in contrast to the anisotropic distortion present in $Pr_{1/2}Ca_{1/2}MnO_3$. Similar evolution of the cell parameters was also reported in the parent compound $Pr_{0.7}Ca_{0.3}MnO_3$ [162] as obtained from SXRPD (Synchrotron X-Rays powder diffraction).

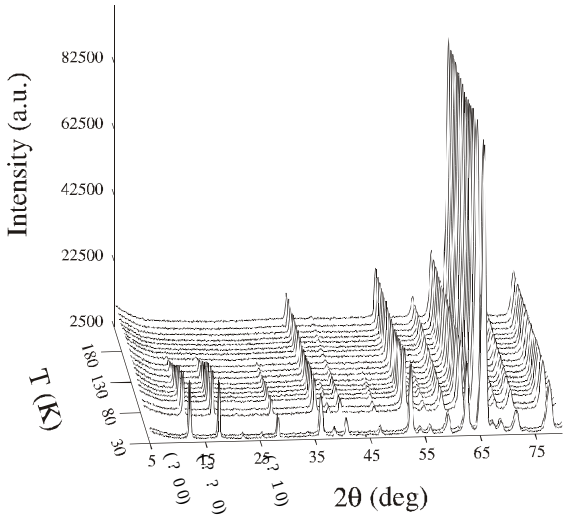

Fig. 7-11 *Thermal evolution of the NPD patterns of the $Pr_{2/3}Ca_{13}MnO_3$ compound where it is possible to observe the onset of AFM order at T_N=150K*

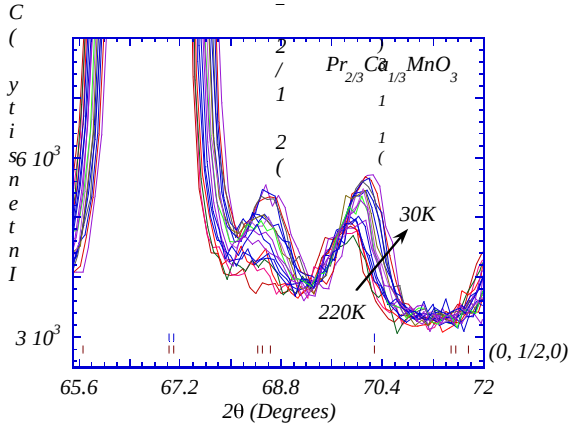

Fig. 7-12 *Evolution of the (2 1/2 0) superstructure peaks appearing at T_{CO} which corresponds to a cell doubled in the b direction in the Pbnm setting.*

The existence of orbital and charge ordering is confirmed by the apparition of a structural modulation below T_{CO}. One superlattice peak is observed in the NPD patterns which has been identified as (2 1/2 2) reflection which suggests a propagation vector: κ=(0,1/2,0) (Fig. 7-12).

Hence, in $Pr_{2/3}Ca_{1/3}MnO_3$ we found similar OO as in x=1/2. However, if the OO, characterised by the doubling of the unit cell in one of the in-plane cell parameters (Pbnm setting) characteristic of the x=1/2 samples, appeared without disorder in the x=1/3 compound, we would expect a highly anisotropic evolution of the cell parameters. No such evolution is observed (Fig. 7-13). Probably disorder does not allow a pronounced lattice deformation similar to that of $Pr_{1/2}Ca_{1/2}MnO_3$. For

example, a possibility is that the excess of e_g electrons instead of occupying the d_z^2 orbitals in the *ab* plane, may be oriented perpendicular to this plane. In this case the *c* lattice parameter would not contract as expected upon cooling through T_{CO}.

Around 155K a series of new peaks at low angles appear as shown in Fig. 7-11. These magnetic peaks are indexed with a magnetic cell $2a \times 2b \times c$ and correspond to a pseudo CE-type AFM structure (Fig. 7-14). The perfect order of this magnetic arrangement can only be achieved when the fractions of Mn^{+3} and Mn^{+4} are equal (x=1/2). The pseudo-CE magnetic structure is closely related to the CE structure but while the magnetic coupling in the CE type structure is AF in the *c* direction, in the pseudo-CE it is FM.

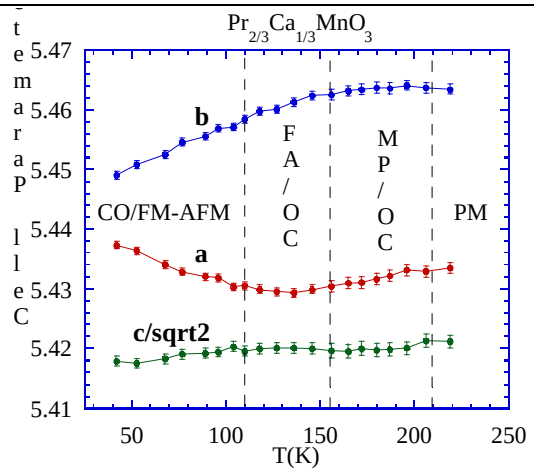

Fig. 7-13 *Thermal evolution of the lattice parameters of $Pr_{2/3}Ca_{1/3}MnO_3$ powder compound as extracted from Rietveld analysis of the medium resolution NPD data (one phase refinement in Pbnm setting).*

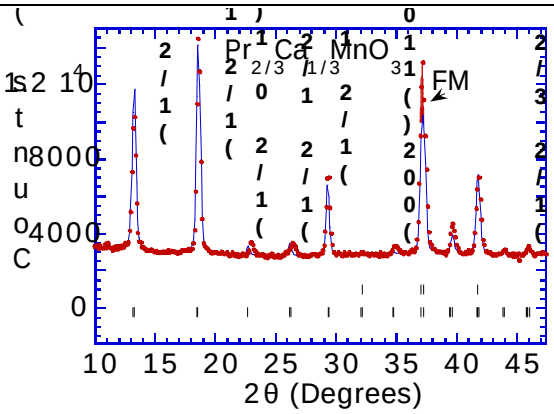

Fig. 7-14 *Low angle detail of the NPD data illustrating the width of the main magnetic peaks at 30K.*

The development of such magnetic coupling may arise from the existence of larger number of long bonds in the *c* direction which accommodate the excess of e_g electrons in x=1/3 doping with respect to the commensurate x=1/2 doping [162]. In Fig. 7-14 can also be observed the existence of tiny (1/2 0 1) and (1/2 1/2 1) intensities characteristic of the CE magnetic ordering suggesting that there is a small fraction of cells with the *ab* planes coupled AFM in the *c* direction.

The AFM peaks are rather narrow in $Pr_{2/3}Ca_{1/3}MnO_3$ compound suggesting that the correlation length of the magnetic order is large. The correlation length ($\xi=\kappa^{-1}$) can be estimated from the FWHM considering that the instrumental peak broadening is smaller than the intrinsic peak broadening. In this case, the correlation length can be obtained from the fit of the experimental peak intensity to a lorentzian function of the type:

$$I = I_{\max} \frac{(\pi k)^2}{(\pi k)^2 + (Q - Q_0)^2} \qquad \textbf{Eq. 7-1}$$

where $2\pi k$ corresponds to the width of the peak and the correlation length extracted corresponds to $\xi(\text{Å}) = \kappa^{-1}$. In the case of the x=1/3 sample the AFM peaks displayed values of the correlation length about 1.8 times larger than the (1/2 0 1) magnetic reflection associated to the Mn^{+3} AFM Bragg peak in the x=1/2 compound. That leads us conclude that the AFM domains in x=1/3 have larger coherence than in x=1/2 compound.

Below ≈120K the integrated intensity of some nuclear reflections (for instance, (0 2 0) and (0 0 2)) are suddenly enlarged indicating the onset of some FM order.

The FM order contribution is mainly observed in the (002) and (110) Bragg reflections (Fig. 7-14). The FM contribution to the peak intensity does not appear as diffuse scattering, but as Bragg intensity, thus meaning that the FM domains are also large. The estimated coherence length of the FM domains is of some hundreds of Å.

In Fig. 7-15 is shown the thermal evolution of the integrated neutron diffraction intensity of some peaks, which are indexed referred to the Pbnm setting. The Fig. 7-15 (a) shows the intensity of the (2 1/2 2) superlattice reflection displayed in Fig. 7-12. The thermal evolution of this superlattice peak gives a definitive evidence of the development of charge ordered regions in the sample below 200K. The magnetic reflections (1/2 0 0) and (1/2 1/2 0) appear at T_N≈150K as shown in Fig. 7-15 (b). Fig. 7-15 (c) and (d) display the integrated intensity of the (0 0 2) and (0 2 0) Bragg peaks which display the onset of long range FM order below T_C=120K.

It should be noted that the superlattice reflection (2 1/2 2) systematically increases upon cooling below T_{CO} without any variation at T_N or T_C, thus suggesting that the crystallisation of the CO regions is apparently unaffected by the appearance of static FM moments in the sample.

Similar conclusions can be extracted from the thermal evolution of the AFM peaks. In this sense, the evolution of the AFM (1/2 0 0) or (1/2 1/2 0) peaks is not altered by the freezing of the FM components Fig. 7-15(b) (d). Hence, the spin reorientation, from collinear CE AFM structure to canted AFM structure, should be ruled out in this system.

Our results suggest the coexistence of two separated magnetic regions. This picture is consistent with some recent studies on $Pr_{0.7}Ca_{0.3}MnO_3$ which reported the observation of large FM droplets [161, 162].

Analysing the NPD data, we attempted to use two different structural phases in the Rietveld NPD refinement. The refinement did not improve significantly the reliability factor (R_{wp}=8.4%) and no clear convergence towards two well-defined set of lattice parameters was obtained. The FM moment obtained from this refinement was m_{FM}=1.5(3) μ_B/Mn and the values of m_{AFM}(I)=1.9(2)μ_B/Mn and m_{AFM}(II)=1.5(3)μ_B/Mn were obtained. When using only one nuclear phase the obtained moments are Mn(I)=2.5μ_B/Mn and Mn(II)=2.3μ_B/Mn which is clearly below the expected values (3.3μ_B for

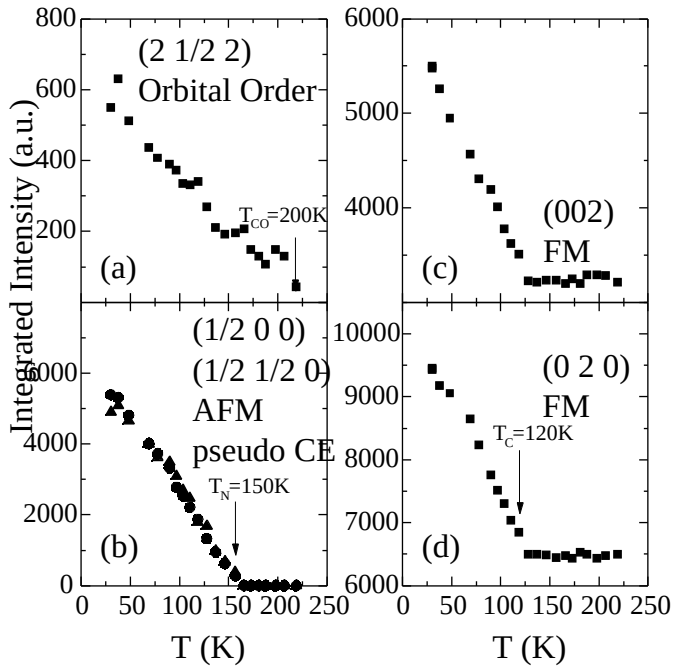

Fig. 7-15 *Thermal evolution of the integrated intensities for (a) (2 1/2 2) CO superlattice, (b) (_ 0 0) and (_ _ 0) AFM CE (c)and (d) (0 0 2) and (0 2 0) which have contribution from the FM ordering (Pbnm setting)*

Mn^{+4} and $4\mu_B$ for Mn^{+3}). In addition, partial FM moment $\mu_{Pr}=0.4\mu_B$ at Pr site has been reported to improve the refinements below 30K [162]. In this case Pr moments are found to be aligned with Mn FM moment. The thermal evolution of the FM and AFM ordered moments is sketched in Fig. 7-16. The low values of the ordered moments obtained Mn(I) and Mn(II) ions sites may be an indication of the existence of phase separation.

7.2.4 Conclusions

In conclusion, our NPD study permitted to identify the presence an orbitally ordered state below T_{CO}=200K which induces a structural modulation with a κ=(0,1/2,0) in the $Pr_{2/3}Ca_{1/3}MnO_3$ compound. This structural modulation is unusual for electron concentration different from n=1/2 and is usually accompanied by an characteristic and sharp anisotropic deformation of the lattice which is absent in the present compound.

However, the low temperature magnetic order of this compound has been identified as a pseudo-CE magnetic structure. This kind of magnetic structure is associated to compounds

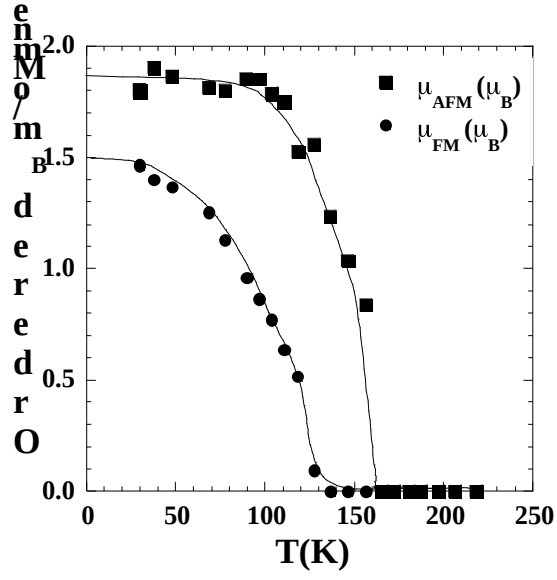

Fig. 7-16 *Thermal evolution of the FM and pseudo-CE AFM magnetic moment.*

exhibiting a slight off stoichiometry of the x=1/2 doping. In addition, a net FM component has been found below 100K.

The thermal evolution of the integrated intensities associated to orbital, AFM and FM order revealed that the crystallisation process of CO regions is unaffected by the onset of static FM moments in the sample. This fact reveals that the low temperature FM moment does not appear from a canting of the existing AFM structure. AFM and FM seem to evolve independently which could be an indication of the existence of two different regions in the sample associated to the AFM and FM order.

However, no evidence of two nuclear phases could be observed even if one of them would be orbitally ordered its unit cell would be highly anisotropically distorted. In addition, the observation of the (2 1/2 2) superlattice peak and the narrow magnetic peaks reveal long-range magnetic and orbital order which would be in contradiction with the existence of two different nuclear structures

In the following section we will characterise the stability under field of the low temperature CO state for the x=1/2 and x=1/3 $Pr_{1-x}Ca_xMnO_3$ compounds. In general, the CO state in x=1/2 Ca doped compound is rather strong and large magnetic fields are needed to melt the charge ordering. The strength of the OO can be characterised by the magnetic fields needed to break the OO. In this sense, a systematic study on the Ca doped compounds with x=1/2 [173] shows that the critical magnetic fields obtained scale rather well with the Mn-O-Mn bond angle in the $Ln_{1/2}Ca_{1/2}MnO_3$ series.

7.3 Stability of the Charge Ordering state under magnetic field

Under a high magnetic field, the induced polarisation of the electronic spins in CO compound competes with the localisation of the charges and favours the delocalisation. A high magnetic field study of the charge ordering melting (electron order to electron disorder transition) on powders of $Pr_{1-x}Ca_xMnO_3$ samples with x=1/2 and 1/3 has been performed at the facilities of the Laboratory SNCMP in Toulouse, France, between 4.2K and 300K. The magnetic fields are obtained using the discharge of a capacitor bank in a resistive coil. Pulsed magnetic fields up to 50T are obtained with pulse duration of about 0.6s (Fig. 7-17).

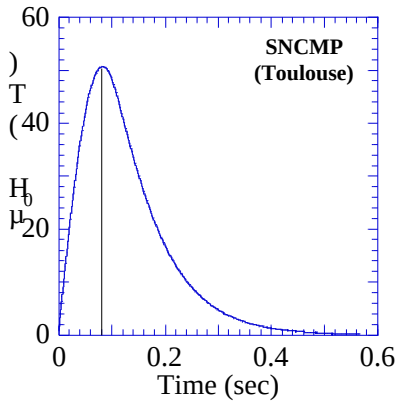

Fig. 7-17 *Time evolution of the magnetic field pulse at SNCMP (Toulouse)*

7.3.1 $Pr_{1/2}Ca_{1/2}MnO_3$

Typical M(H) curves obtained on $Pr_{1/2}Ca_{1/2}MnO_3$ for selected temperatures are shown in Fig. 7-18. Isothermal magnetisation measurements were always performed after zero field cooling process in order to obtain the virgin magnetisation curves.

M(H) curves obtained below T_{CO}≈230K in $Pr_{1/2}Ca_{1/2}MnO_3$ polycrystalline sample display hysteresis which is characteristic feature of the first order character of the charge-order to charge-disorder transition. The melting of charge ordering under applied magnetic field implies a concomitant structural and insulator-to-metal transitions. The spontaneous magnetisation in the melted state is estimated to be $3.7\mu_B$/Mn and confirms that the obtained phase is fully FM.

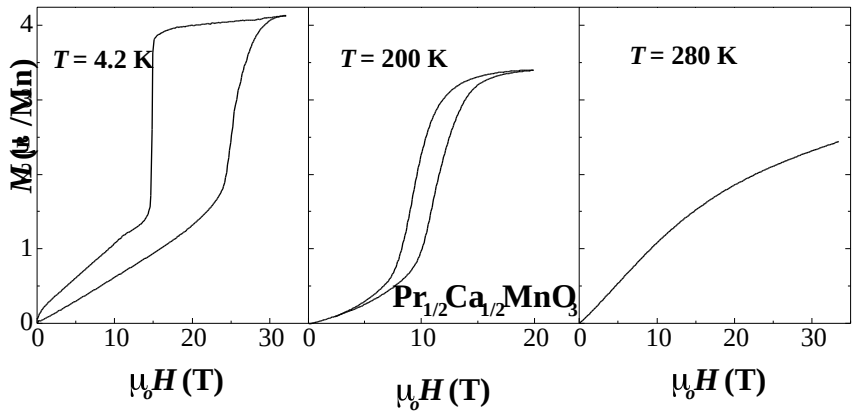

Fig. 7-18 *Magnetisation versus field curves for $Pr_{1/2}Ca_{1/2}MnO_3$ powders measured at 4.2K (below T_N), 200K (above T_N=180K) and 280K (aboveT_{CO}=230K)*

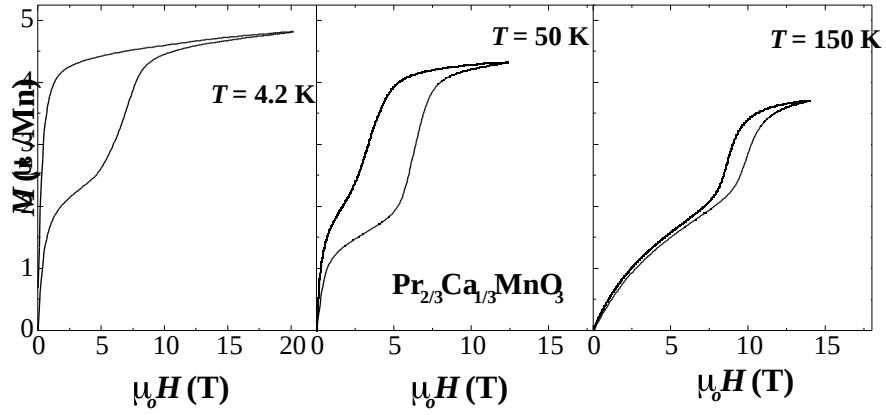

Fig. 7-19 *Magnetisation versus field curves for $Pr_{2/3}Ca_{1/3}MnO_3$ powders measured at 4.2K (below T_C), 50K (above T_{Pr}) and 150K (above T_C=100K and below T_{CO}=230K)*

Critical fields are defined as $\mu_0 H_C^+$ and $\mu_0 H_C^-$, and correspond to the inflexion point of the hysteresis loops with an increasing (+) or decreasing (-) magnetic field sweeps. No corrections related to demagnetising fields have been performed but considering the powdered sample as being formed by spherical particles, the field inside the particle would be reduced by 1/3 of the magnetisation. The thermodynamic transition field is defined as the averaged field between $\mu_0 H_C^+$ and $\mu_0 H_C^-$.

7.3.2 $Pr_{2/3}Ca_{1/3}MnO_3$

Similar M(H) measurements have been performed on $Pr_{2/3}Ca_{1/3}MnO_3$ polycrystalline samples (Fig. 7-18). The spontaneous magnetisation in the melted state also corresponds to a fully FM state. Moreover, at 4K the spontaneous magnetisation is about $4.4\mu_B$/Mn which is larger than the value expected for the spin-only moment ($3.66\mu_B$/Mn). At 50K the spontaneous magnetisation is slightly smaller ($4\mu_B$/Mn) than at 4K which suggest the possibility of FM alignment of Pr moment at 4K. However, it can be observed that, at any temperature below $T_{CO,}$ this compound exhibits larger susceptibility for low fields in contrast with the x=1/2 compound. This can be a signature of the existence of FM components or phases, which align under the application of a magnetic field. On the other hand, $\mu_0 H_C^-$ and $\mu_0 H_C^+$ in x=1/3 compound are smaller than in the case of $Pr_{1/2}Ca_{1/2}MnO_3$ and there appears some remanence at low temperatures.

There exists a large hysteresis between the increasing field and decreasing fields sweeps in both samples (x=1/2, x=1/3) and the hysteresis becomes broader at low temperatures (T<30K). It is a signature of the first order character of the CO-CD (charge disordered) transition: thermal relaxation between two possible states that constitute local minima, are strongly suppressed when the thermal energy is reduced upon cooling below certain temperature.

The obtained thermodynamic critical fields at 4K of 3.6T in x=1/3 and 22T in x=1/2 are very different and reveal that even if the orbital order in x=1/3 has been found to be the same than in x=1/2 compounds, the excess of electrons in this compound may be at the origin of the weakening of the stability of the OO and of the development of static FM order at low temperatures.

In addition to that, it has been experimentally observed that the thermodynamic critical field scales with the Mn-O-Mn mean angle in the $Ln_{1-x}Ca_{1/2}MnO_3$ series [173]. In the case of the $Pr_{1-x}Ca_xMnO_3$ series, the two atoms shearing the A-site in the structure have very similar radii (1.126Å [Pr^{+3}] and 1.12[Ca^{+2}]). For that reason, local strain effects coming from the size distribution of the A-site cations are minimised in $Pr_{1-x}Ca_xMnO_3$ compounds. Hence, the presence of magnetic inhomogeneities in this case should be ascribed to an inhomogeneous ground state at the microscopic level.

T-H phase diagrams have been constructed from the determination of the critical fields obtained from the M(H) curves at several temperatures and are shown in Fig. 7-20. Remarkable differences are observed when comparing the T-H phase diagrams of $Pr_{1/2}Ca_{1/2}MnO_3$ and $Pr_{2/3}Ca_{!/3}MnO_3$ compounds. A striking feature is that $\frac{\partial H_C^+}{\partial T} > 0$ for $Pr_{2/3}Ca_{!/3}MnO_3$ in the temperature interval 150K>T>50K. This unexpected behaviour is in contrast with the usual sign $\frac{\partial H_C^+}{\partial T} < 0$ for $Pr_{1/2}Ca_{!/2}MnO_3$. Hence, a reentrant like behaviour occurs in x=1/3 compound. Similar reentrant like behaviour has been reported for the x=0.45 and x=0.40 doping levels [174]. The reentrant like behaviour can be explained considering that for hole doping slightly below x=1/2, the system with short range repulsion is unstable and tends to the phase separation. However, long-range Coulomb forces would prevent the formation of large regions consisting in CE-type CO regions containing a density of electrons close to n=1/2 and the other containing the excess of electrons and some holes and thus being metallic.

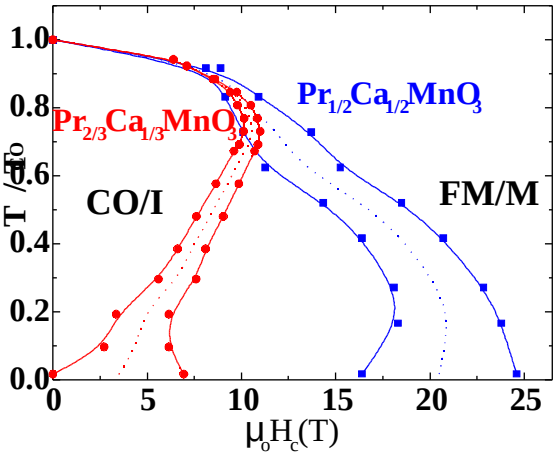

Fig. 7-20 *Phase diagram of $Pr_{1-x}Ca_xMnO_3$ compounds for x=1/2 and x=1/3 obtained from magnetisation measurements.*

In conclusion, high magnetic field study agrees with the idea that the excess of electrons which do not contribute to favour the OO in x=1/3 compound, do contribute to enhance the FM coupling in the pseudo-CE magnetic structure and diminish the critical fields for the CO melting.

On the other hand, the large susceptibility at low magnetic fields of x=1/3 compared with x=1/2 compound that develops below T_C is an indication of the existence of FM regions in the sample. In addition to that, the onset of the slope change from $\frac{\partial H_C^+}{\partial T} > 0$ to $\frac{\partial H_C^+}{\partial T} < 0$ in x=1/3 occurs well above T_C (approximately

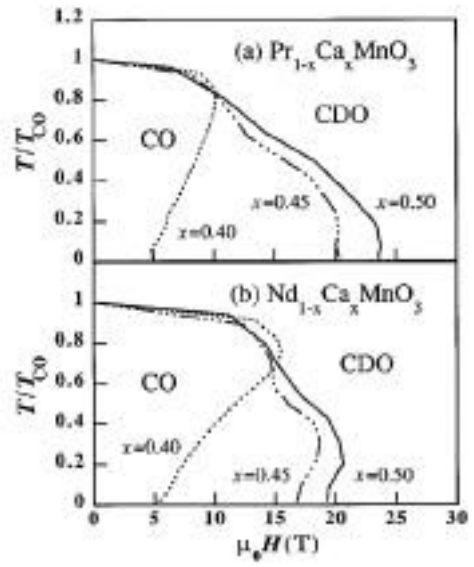

Fig. 7-21 *Temperature dependence of the thermodynamic transition fields in $Pr_{1-x}Ca_xMnO_3$ and $Nd_{1-x}Ca_xMnO_3$ as extracted from* [174]

at T_N) so if not such FM correlations existed in the whole temperature range, or appeared only around T_C, the slope change would be only expected below T_C.

Hence, from high magnetic field study and NPD experiments we rule out the possibility of having an homogeneously canted AFM state at temperatures below T_{CO}. The nature of such low temperature ground state could not be defined from our NPD studies nor SXRPD [162] because only one lattice is observed which has been found to develop a $\kappa=(0,1/2,0)$ structural modulation characteristic of commensurate x=1/2 CO compounds.

To go further in the understanding of the nature of the coexisting long range FM and CO we have used a local probe technique as μSR that we describe in the following chapter.

7.4 μSR study of the Charge Ordering and phase segregation

One of the purposes of the present section is to use a local magnetic probe to give insight into the real spatial distribution of the FM ordered regions with respect to the AFM coupled charge-ordered zones. With this objective in mind Zero Field μSR spectra were collected in zero external applied field (ZF) over the temperature range 15-300K. ZF-μSR allows the study of the spin dynamics in zero applied fields in contrast to other techniques like NMR or EPR.

In the following section, we recall the basis of ZF-Muon Spin Relaxation technique.

7.4.1 Introduction to Muon Spin Relaxation (μSR)

Muons are fundamental fermions and belong together with the electron and tauon to the group of charged leptons. Muons have spin 1/2, carry one elementary electric charge (positive o negative), and have a mass about 207 times the rest mass of the electron or 1/9th of the proton rest mass. Thus, from a particle-physics point of view, they are "heavy electrons", whereas from a solid-state-physics or chemistry point of view they are "light protons".

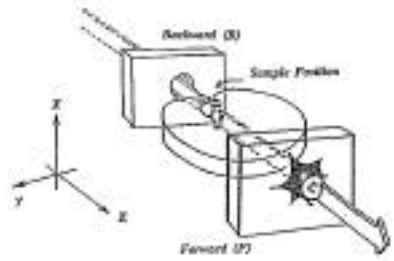

Fig. 7-22 *Schematic representation of a ZF-μSR experiment*

In a standard ZF-μSR experiment a beam of positive muons with negative helicity and fully spin polarised along the beam direction is stopped in a target specimen (Fig. 7-22). Muons thermalise in the specimen where they are implanted very quickly (10^{-12}s) and the muon spin processes in the local field at its particular site with a frequency $\upsilon=(\gamma_\mu/2\pi)B$ (muon gyromagnetic ratio $\gamma_\mu/2\pi$=13.553kHz/G).

Some times the positive muon, μ^+, forms a bond state with the electrons (muonium) of the system but this bounding has not been observed in metals nor in oxides and thus in such materials μ^+ behave as free particles.

Muons decay into a positron (τ_μ=2.2μs, $\tau_\mu\nu$=0.03 G^{-1}*B) and two neutrinos and because of the parity violation of the weak interaction, the positron is preferentially emitted along the muon-spin direction (Fig. 7-23) with a probability function of the type $W(\theta)=1+a\cos(\theta)$, being θ the angle between the muon spin direction and the positron emission.

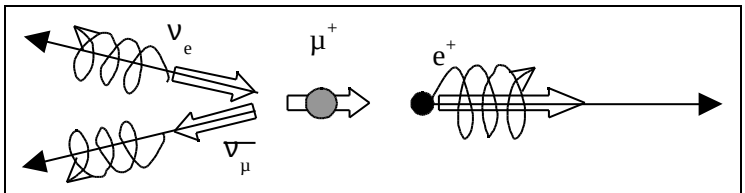

Fig. 7-23 *Positive muon decay*

Positron detection is used to establish the time and direction of the muon spin at the instant of decay. The time histograms of the accumulated positron in opposing counters (Fig. 7-22), $N_{B,F}(t)$ (B stands for backward and F for forward) reflect the muon local fields:

$$N_{B,F} = B_{B,F} + N_0 \exp\left(-\frac{t}{\tau_\mu}\right)\varepsilon_{B,F}\left[1 \pm A_{B,F}G_z(t)\right] \qquad \textbf{Eq. 7-2}$$

where N_0 is a normalisation factor, $\varepsilon_{B,F}$ is the positron detector efficiency, $B_{B,F}$ is the beam-borne background in the detector, $A_{B,F}$ is the intrinsic asymmetry of the positron detectors ($A\approx0.25$ is a geometrical parameter) and $G_z(t)$ is the muon spin relaxation function along the z axis. The time evolution of $G_z(t)$ reflects the amplitudes, randomness, and fluctuations of local magnetic fields at muon sites in the specimen. In a pulsed source $B_{B,F}$ is very small and the experimental asymmetry is obtained as:

$$a_0(t) = \frac{[N_B(t) - B_B] - [N_F(t) - B_F]}{[N_B(t) - B_B] + [N_F(t) - B_F]} \approx \frac{N_B(t) - \alpha N_F(t)}{N_B(t) + \alpha N_F(t)} = a_0 G_z(t) \qquad \textbf{Eq. 7-3}$$

where α is a calibration parameter ($\alpha\approx1$) and is experimentally determined from a fit of the oscillations in Ag under a low applied magnetic field (2-4mT).

The local internal magnetic fields at the muon sites originated from dipolar interaction with surrounding nuclear or electronic spins, as well as contact hyperfine fields from the spin density at the muon site depolarise the muon.

The internal field from spins in the long range ordered state of regular FM or AFM tends to be unique in magnitude with a particular direction with respect to the crystal lattice. Multiple muon sites in a unit cell or crystallographically equivalent but magnetically inequivalent muon sites could

result in multiple magnitudes of such field. In the case of a static local magnetic field, *H*, at the muon site, de depolarisation function is:

$$G_z(t) = \int d^3H\ P(H_x, H_y, H_z)\left(\frac{H_z^2 + (H_x^2 + H_y^2)\cos(\gamma_\mu H t)}{H^2}\right) \qquad \textbf{Eq. 7-4}$$

P(H) is the magnetic local field distribution at the muon site. Depending on the local field distribution function P(H), different depolarisation functions are obtained.

In the absence of an external applied field, the oscillating frequency of $G_z(t)$ is proportional to the magnetic order parameter M. More information about the technique can be found in [175-178].

7.4.2 ZF-μSR study on $Pr_{1-x}Ca_xMnO_3$ (x=1/2 and x=1/3)

Experiment

We have performed a series of ZF-μSR measurements at ISIS pulsed muon facility in the Rutherford Appleton Laboratory (UK) using MUSR instrument on $Pr_{1-x}Ca_XMnO_3$ (x=1/2 and x=1/3) polycrystalline samples. The ISIS synchrotron produces a beam of protons, which is pulsed with a repetition rate of 50 Hz. In fact, each pulse is actually made up of two proton bunches each with a width of approximately 70 ns and a separation of 300 ns. The muons produced at the graphite target have a similar time structure, slightly smeared out due to the 26 ns pion half-life (Fig. 7-24).

In pulsed sources as ISIS, it is possible to investigate slow spin fluctuations and small internal fields (H<6mT) because of the fast decay of the asymmetry and the impossibility to observe the oscillations of the asymmetry function when the internal field is too high. This is because the muon pulse has a width of about 70ns and imposes a reduced frequency window.

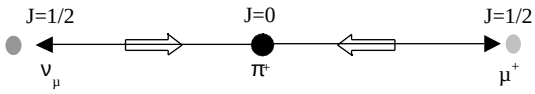

Fig. 7-24 *Pion decay in the pion rest frame. The fixed helicity of the ν_μ, J conservation, and momentum conservation forces the muon to have negative helicity.*

A 10g powder samples were mounted on an Al plate with a silver mask in a closed circuit refrigerator, and the measurements were made in the temperature range 15-350K. Longitudinal fields up to 0.2T were also applied at several temperatures without changes in the relaxation time. This suggests that the muon depolarisation is not produced by the static random nuclear moments but the fluctuating electronic moments.

In the perovskite structure, the muons are most likely to be located close to the oxygen anions due to their high affinity to form O-μ^+ bond [179]. Unlike previous studies in orthoferrites, studies on the parent compound $La_{2/3}Ca_{1/3}MnO_3$ [28] showed no evidence of multiple stopping sites or muon diffusion in the temperature range 1.5K-300K. We found no evidence of muon diffusion in Pr-Ca-

MnO_3 (x=1/2, x=1/3) in the temperature range of the present study. Hence, possible effects due to muon diffusion can be neglected in the present study.

Above T_N, the relaxation function, $G_z(t)$, for the $Pr_{1-x}Ca_xMnO_3$ (x=1/2 and 1/3) can be described with a single exponential decay corresponding to fast fluctuating fields :

$$G_z(t) = a_0 \exp(-\lambda t) \qquad \textbf{Eq. 7-5}$$

where a_0 is the initial asymmetry and λ is the dynamic spin-lattice relaxation rate (or damping rate). The latter is proportional to the amplitude of the fluctuating local magnetic field (B_{loc}) acting at the muon site and created by neighbouring magnetic ions through dipolar coupling. The damping rate is also proportional to the correlation time that characterises the fluctuations:

$$\lambda = \gamma_\mu^2 \langle B_{loc}^2(0) \rangle \tau_c \qquad \textbf{Eq. 7-6}$$

being $\gamma_\mu = 2\pi \times 13.55$ kHz/Oe (gyromagnetic ratio of the μ^+), τ_c the primary correlation time between the fluctuations and the angular brackets the static equilibrium average of the square of the local magnetic field at the μ^+ site. The local magnetic field at the muon site arises from the sum of a hyperfine field B_{hyp} and a local dipolar field B_{dip}. In oxides, where the muon is found to be close to the oxygen atom, the hyperfine field is in part due to the formation of an muon-oxygen covalent bond [180]. In orthoferrites and cuprates was found that $B_{hyp} << B_{dip}$ so it seems reasonable to assume that B_{hyp} is also negligible in manganites. In addition, hyperfine coupling is very small in non metallic compounds as is the case of the compounds in our study.

Below the ordering magnetic transition, the initial asymmetry, a_0, reduces to 1/3 of its value at higher temperature. This is because the appearance of a spontaneous non-zero static fields causes precession of the muon spin and the subsequent muon spin rotation falls beyond the accessible frequency window at ISIS. Hence, when there is static magnetic order, only the component of the muon polarisation parallel to the local magnetisation preserved and this is the measured component in ZF-μSR. When integrating over all directions in a multidomain or powder sample the component is 1/3.

Below T_N=170K a stretched exponential (SE) function is required to describe the muon decay:

$$G_z(t) \approx \exp(-\lambda_S t)^\beta \qquad \textbf{Eq. 7-7}$$

Stretched exponential (SE) function is usually found in spin glass systems [181] [182]. $\beta<1$ when there exist a distribution of λ and that means that there is a distribution of correlation times, τ_C, and/or local fields B_{loc}. We use it to describe the ordered state because within the accuracy of our data, it describes the data at low temperatures rather well but we do not attempt to give further interpretation of the significance of β in the ordered state of our samples.

Typically, near a magnetic phase transition the correlation time becomes longer, causing λ to increase, a phenomenon known as "critical slowing down" of the magnetic fluctuations. The temperature dependence of the relaxation rate in the critical regime ($0.99T_C<T<T_C$) of a second order magnetic phase transition can be parameterised by a power law [183, 184] of the form:

$$\lambda = D\left(\frac{T - T_C}{T_C}\right)^{-\omega} \qquad \textbf{Eq. 7-8}$$

where ω is the dynamic critical exponent and D is a proportionality constant. Below the ordering temperature, the fluctuating amplitude decreases and λ is reduced.

In the following section, the behaviour of the μ^+ spin depolarisation characteristic of a CO compound with x=1/2 doping level is sketched and will be compared to the x=1/3 compound.

7.4.2.1 $Pr_{1/2}Ca_{1/2}MnO_3$: An example of x=1/2 CO compound

In Fig. 7-25 is shown the measured μSR relaxation functions $G_z(t)$ at several temperatures for the $Pr_{1/2}Ca_{1/2}MnO_3$ compound. In the figure it can be observed the fast drop of the initial asymmetry at the magnetic ordering temperature (T_N=180K) while at the CO temperature (T_{CO}=230K) the initial asymmetry do not change.

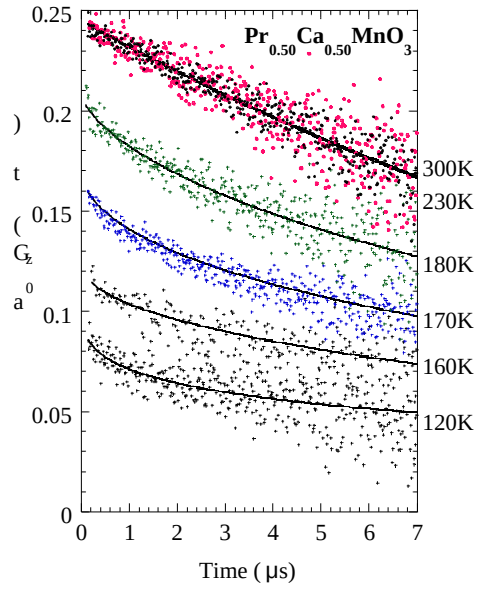

Fig. 7-25 *Time dependence of the ZF muon relaxation spectra of $Pr_{1/2}Ca_{1/2}MnO_3$ at some selected temperatures.*

The obtained thermal evolution of the initial asymmetry and relaxation rate extracted from our data analysis using the expressions of the muon depolarisation function explained in the above section, are shown in Fig. 7-26. Upon cooling, the initial asymmetry displays a drop at T_N and does not exhibit any feature at T_{CO} suggesting that there exists no magnetic ordering in the temperature range between T_{CO} and T_N, and the sample remains in the PM state.

The relaxation rate, λ, shows a relative maximum when cooling through the charge ordering temperature. This change of slope is associated to the reduction of the coupling strength between muon and electron spins. Its origin is the substitution of FM by AFM interactions in the Mn sublattice. As the temperature goes down further in the PM phase, the exponential damping rate displays a minimum and then increases again as the fluctuations slow down towards the Néel point.

We have also observed the maximum in the relaxation rate close to T_{CO} in other samples with perfect 1:1 electron/hole (Mn^{+3}/Mn^{+4}=1, x=1/2) proportion exhibiting CO [185] indicating that this behaviour is characterises the CO transition.

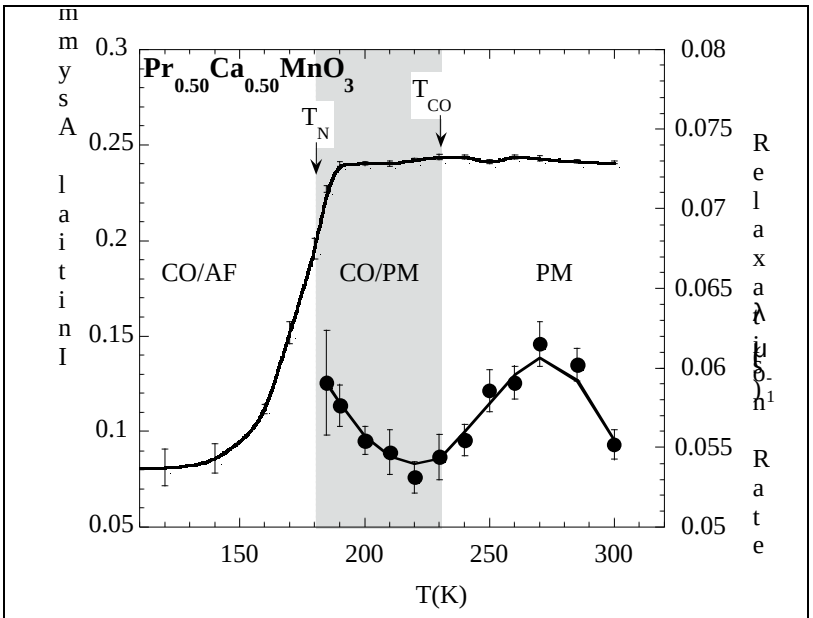

Fig. 7-26 *Temperature dependence (warming) of the μ^+SR initial asymmetry and the relaxation rate for $Pr_{1/2}Ca_{1/2}MnO_3$*

7.4.2.2 Pr2/3Ca1/3MnO3: Study on the phase segregation phenomena

In the following section, we will concentrate on the $Pr_{2/3}Ca_{1/3}MnO_3$ compound in order to elucidate the spatial distribution of the FM ordered regions with respect to the AFM coupled CO regions. We will also examine the CO transition and compare it to the transition exhibited by the x=1/2 compound.

The $Pr_{2/3}Ca_{1/3}MnO_3$ compound, although it exhibits rather similar macroscopic behaviour compare to the x=1/2 compound, it presents differences in the muon spin depolarisation behaviour when compared with the x=1/2 compound.

Above $T_N \approx 155K$ the single exponential decay function characterises the depolarisation of the implanted muons as in the case of the x=1/2 sample and below T_N a stretched exponential function is required to describe the muon decay. In Fig. 7-27 is shown the time dependence of the ZF muon relaxation spectra at several selected temperatures.

The thermal variation of the SE relaxation rate (λ_s) and the initial asymmetry (a_0) obtained from the analysis of the ZF-μSR are shown in Fig. 7-28. The solid line reproducing $\lambda_s(t)$ above the ferromagnetic transition temperature is a fit by the function $\lambda_s \ (T/T_C - 1)^{-\gamma}$ which gives T_C=120(3)K,

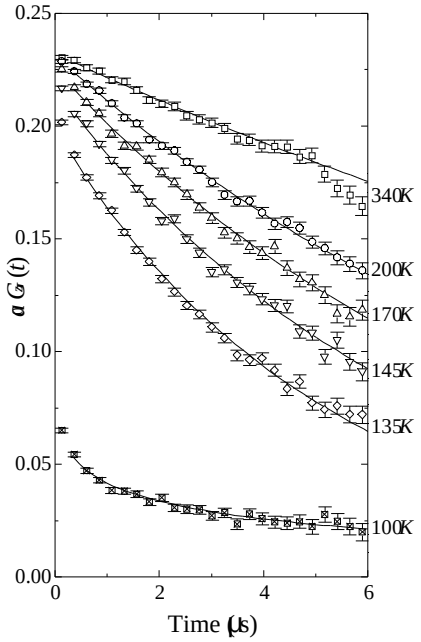

Fig. 7-27 *Time dependence of the ZF muon relaxation spectra at several selected temperatures of the $Pr_{2/3}Ca_{1/3}MnO_3$ powders.*

γ=0.51(1) and λ_0=0.066(1)μs^{-1}. The transition temperature determined by this description agrees well with the determined T_C from magnetisation and neutron measurements. However, the fit was carried out in a larger temperature range than the asymptotic critical regime, and strictly speaking, Eq. 7-8 is only valid in the asymptotic critical region of a second order magnetic phase transition. The obtained value of γ≈1/2 corresponds to the value expected from the mean field approximation.

The fact that the relaxation rate diverges at T_C instead of T_N suggests that the dominant relaxation mechanism of the muon polarisation in this case is based on FM Mn-Mn correlations which seem to be present at any temperature.

We will now focus our attention on the value of the relaxation rate. About the sign of the magnetic interactions, it is important to recall the following systematic features reported in previously μSR literature. In manganites where AFM correlations are dominant (for example, CO x=1/2 compounds) the relaxation rate is always within the interval λ≈0.04-0.06μs^{-1}, even very close but above T_N. But in manganites where the FM correlations dominate, the relaxation rate falls within the interval λ≈0.10-0.30μs^{-1}above T_C [186, 187] [188, 189].

It is then very important to emphasise that the values of the relaxation rates obtained for the x=1/3 sample belong to the characteristic interval for FM samples. Indicating that the muon being effectively depolarised by FM Mn-Mn correlations and for that reason, the thermal evolution of the spin-lattice relaxation rate is peaked at T_C instead of T_N.

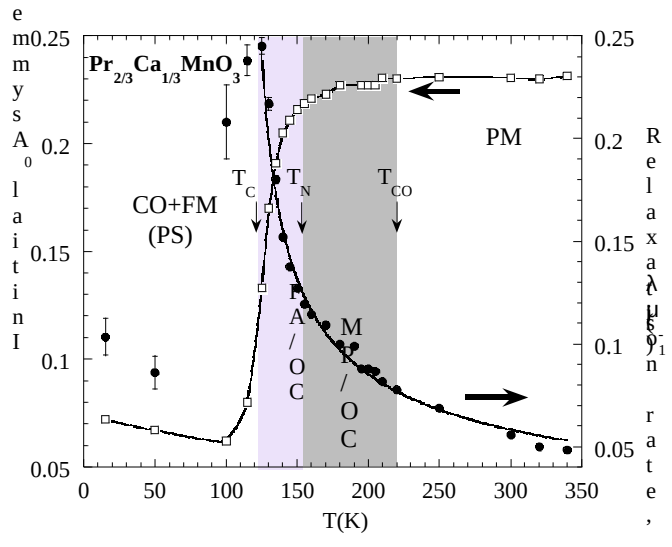

Fig. 7-28 *Thermal evolutions of the relaxation rate and initial asymmetry for $Pr_{2/3}Ca_{1/3}MnO_3$ compound as extracted from the analysis of the ZF-μSR data.*

Another remarkable feature is the evolution of the initial asymmetry in this x=1/3 compound. The initial asymmetry begins to drop at T_N but the abrupt reduction is at T_C indicating that below T_N the whole sample do not display static magnetic order.

Finally, a remarkable finding is that λ(t) does not display any particular feature at T_{CO} as in x=1/2 CO samples and observed in $Pr_{1/2}Ca_{1/2}MnO_3$ compound [185, 186].

In the following section we will give an image of the inhomogeneous ground state in $Pr_{2/3}Ca_{1/2}MnO_3$ compound from the light of the μSR, NPD analysis and high field magnetisation measurements

7.5 Discussion and conclusions

Several remarkable differences have been observed in the structural evolution, magnetic structure at low temperature, critical magnetic fields and in the μSR depolarisation behaviour between the compounds $Pr_{1-X}Ca_XMnO_3$ with x=1/3 and 1/2. The main point in this discussion is to find out and describe the low temperature phase of the x=1/3 compound which exhibits an orbital order characteristic of an x=1/2 sample and develops static FM order at low temperatures.

The three possible scenarios which could describe the low temperature phase in $Pr_{2/3}Ca_{1/3}MnO_3$ are:

a) The first scenario is the simplest one. It proposes to consider the low temperature phase as an homogeneous canted AFM having its origin in a spin rearrangement below T_C=120K.

b) The second scenario consists in an inhomogeneous low temperature configuration with CO regions forming large domains of coherence, AFM ordered and spatially separated by FM domains or large clusters. The last probably displaying a distribution of sizes. In the framework of “phase separation” models, the FM regions are richer in e_g electrons than the CO ones.

c) The third scenario consists in an inhomogeneous ordered phase where AFM and FM regions have a spatial distribution strongly overlapped in such a way that variable size clusters of the FM phase are densely scattered within the CO phase and occupy a large fraction of the sample.

The first scenario of a homogeneous low temperature canted AFM state originated from the spin rearrangement of the Mn moments below T_C can be ruled out from the inspection of the thermal evolution of the AFM and FM moments obtained from NPD (Fig. 7-16). There is no significant coupling between the FM and AFM phases. This is also corroborated by the fact that the CO crystallisation (thermal evolution of the (2 1/2 2) superlattice peak) is not affected by the appearance

of static FM moments. In addition, μSR data have established that the FM interactions do exist in the whole temperature range, even well above T_N and T_{CO}

The second scenario, consisting in CO-AFM regions with large isotropic domains of coherence and spatially separated by FM domains, also disagrees with the experimental data and is highly improbable because long range Coulomb forces would prevent the full phase separation into large regions containing the extra electrons and the n=1/2 CO region. In the second scenario, we would also expect to observe two different cells: one from the FM domains and another highly anisotropic and exhibiting OO from the CO domains. Not such different cells have been observed by our NPD nor by high resolution SXRPD as reported [162]. One reason for not observing two different cells would be that the FM domains were very small. However, in this case they would not give a coherent FM signal in NPD measurements but would give diffuse contribution. And this is not the case, as extracted from our NPD measurements.

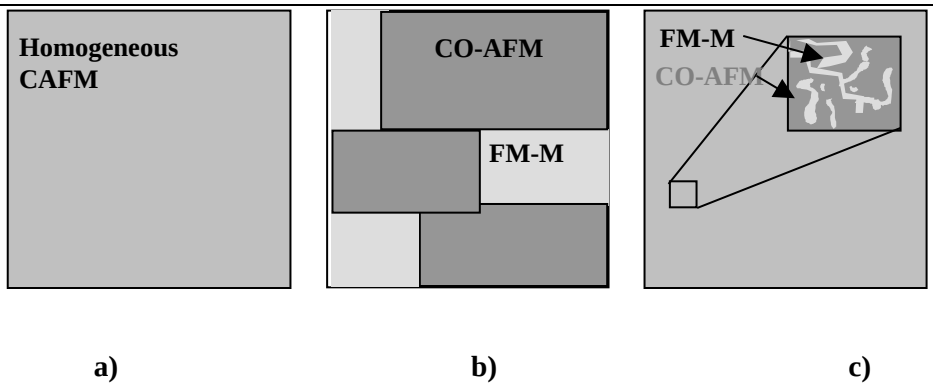

Fig. 7-29 *Schematic representation of the three possible descriptions of the low temperature phase in $Pr_{2/3}Ca_{1/3}MnO_3$*

In addition, even if the size of the individual FM clusters were smaller than the AFM domains, since muons are randomly distributed in the sample, an abrupt reduction of the initial asymmetry would occur at T_N if the AFM domains were a majority phase. In the temperature range $T_C<T<T_N$, a certain proportion of muons would be implanted in fully CO-AFM domains while others would be in PM domains. Thus, a plateau in the initial asymmetry evolution would be expected in this temperature range. Moreover, the drop to 1/3 value would occur at T_C. But not such behaviour is observed in Fig. 7-28 confirming that the FM and AFM regions are not spatially separated but highly interpenetrated. The same conclusion is reached from the lack of local maxima in the thermal evolution of the relaxation rate at T_{CO}.

In Fig. 7-30 is shown the temperature dependence of the relative fraction of muons feeling a local static field at their site as extracted from the thermal evolution of the initial asymmetry of our μSR data. The existence of frozen moments in the whole volume is only attained below T_C=120K in x=1/3 compound while in the case of the x=1/2 compound the process occurs rather faster immediately below T_N. In addition, the apparition of ordered regions is not abrupt at T_N in x=1/3 compound. This behaviour can be ascribed to a distribution of Néel temperatures in the sample with origin at the lattice strain or driven by local fluctuations of the density of e_g electrons.

The stability of the charge order in x=1/3 presents a re-entrant like behaviour at low temperatures which is characteristic of samples presenting off stoichiometry from the Mn^{+3}/Mn^{+4}=1 ratio. In addition, x=1/3 sample displayed larger low field susceptibility which characterises the FM zones.

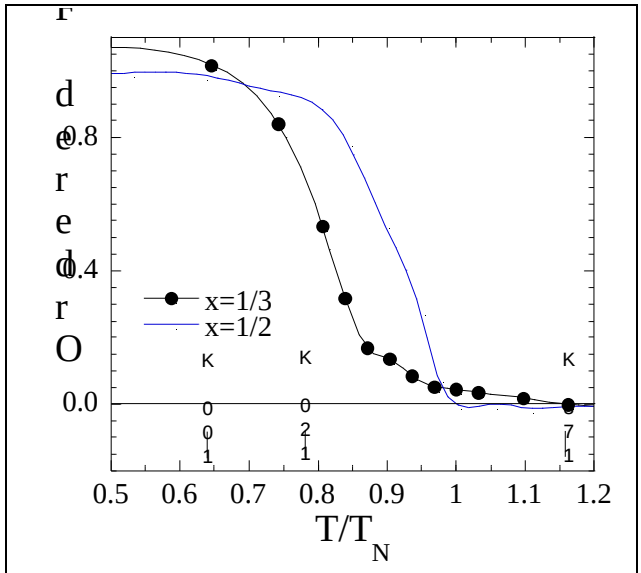

Fig. 7-30 *Thermal dependence of the fraction of muons sensing a static magnetic field for $Pr_{1-x}Ca_xMnO_3$ compounds (x=1/2 and x=1/3) as extracted from ZF-μSR experiments*

In conclusion, we have investigated the coexistence of FM-metallic and AFM-CO phases in $Pr_{2/3}Ca_{1/3}MnO_3$, in comparison with $Pr_{1/2}Ca_{1/2}MnO_3$. μSR data confirms the existence of highly interpenetrated FM (some hundreds of Å) and AFM regions at a microscopic scale in the $Pr_{2/3}Ca_{1/3}MnO_3$ sample at low temperatures. Moreover, although the AFM-CO regions are large (100 to 1000Å), they contain large FM domains densely scattered that can be at the origin of the non-existence of a second nuclear phase characterising the FM phase.

In addition, the existence of zones with no orbital order inside the orbitally ordered zones would prevent the fully development of the anisotropic distortions of the lattice when the structural modulation with propagation vector κ=(0,1/2,0) characterising the OO accompanying the pseudo CE magnetic structure is stabilised. In effect, the x=1/3 sample displays a rather low value of the cell distortion parameter $\varepsilon_c = \left(1 - \frac{\sqrt{2}c}{a+b}\right) \times 10^3 \approx 3$ while for x=1/2 sample the obtained value is 26. This is an indication that the CO regions contain structural defects densely scattered that can be associated to the FM zones.